NUMERICAL ANALYSIS OF WAVE BREAKING DUE TO SUBMERGED BREAKEWATER IN THREE-DIMENSIONAL WAVE FIELD

Koji KAWASAKI¹ and Koichiro IWATA²

ABSTRACT

The wave breaking and post-breaking wave deformation due to a submerged breakwater in a three-dimensional wave field have been investigated numerically and experimentally in this study. The calculated and measured results have revealed that the breaking limit and the breaker types are almost independent of the relative structure length W/L_i (0.5 $\leq W/L_i \leq$ 2.5), and that the horizontal and vertical circulation flows are formed around the submerged breakwater. It is also found that the wave breaking in three-dimensional wave field is affected strongly by the wave refraction, different from the twodimensional case. The numerical calculation method based on a SOLA-VOF method has been developed and has reproduced well laboratory experiments in case of a weak breaker such as the Spilling breaker.

INTRODUCTION

Accurate prediction and evaluation of wave breaking process due to a submerged breakwater are important in view of multi-purpose utilization of coastal sea area as well as the wave dynamics. Researches have ever been conducted to evaluate numerically and experimentally the wave breaking and its deformation due to the submerged breakwater. Most of these researches are, however, limited to a two-dimensional wave field (for examples, Petit et al., 1994; van Gent et al., 1994; Sabeur et al., 1996; Iwata et al., 1996).

The main purpose of this study is to discuss numerically and experimentally the wave breaking process due to a submerged breakwater in a three-

¹⁾ Research Associate, Dept. of Civil Eng., Osaka Univ., Osaka 565-0871, JAPAN

²⁾ Professor, Dept. of Civil Eng., Nagoya Univ., Nagoya 464-8603, JAPAN

dimensional wave field. First, elaborate three-dimensional laboratory experiment was conducted to study the breaking limit, the breaker type, the breaking position and the wave deformation after breaking in the regular wave field, in relation to the relative dimensions of submerged breakwater to the waves. Next, the numerical calculation method based on the SOLA-VOF method (Hirt and Nichols, 1981) is developed to investigate the wave breaking process due to the submerged breakwater. The validity of the present method is verified by comparing with the experimental results.

LABORATORY EXPERIMENTS

Three kinds of laboratory experiments, such as Series I on the breaking limit, breaker type and breaking position, and Series II and III regarding the wave deformation and the water particle velocity field after breaking, were carried out in a three-dimensional wave basin (28m in length, 8m in width and 0.8m in depth) at Nagoya University. In the experiments, the relative width B/L_i , the relative submerged depth R/h and the relative height D/h of the submerged breakwater were fixed as $B/L_i=0.3$, R/h=0.4 and D/h=0.6, where B is the structure width, R the submerged depth, D the structure height, and L_i the wavelength at the still water depth h. The still water depth was kept constant at 40cm. The relative submerged breakwater length W/L_i was as-

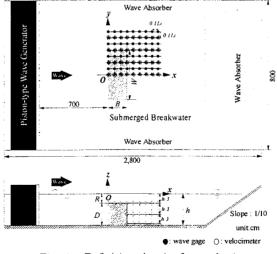


Fig. 1 Definition sketch of wave basin

854

signed as $W/L_i=0.5$, 1.0, 1.5, 2.0 and 2.5. The regular waves with different wave periods $T_i=0.8$, 1.2 and 1.68s were generated so as to propagate perpendicularly to the submerged breakwater. The incident wave height H_i was, in Series I, carefully changed to find out the breaking limit and the breaker types. On the other hand, H_i in Series II and III were chosen so that the following non-linearity parameter Π (Goda, 1983) was 0.08 and 0.09 for three different wave periods.

$$\Pi = \frac{H_i}{L_i} \coth^3\left(\frac{2\pi h}{L_i}\right) \tag{1}$$

Note that the above-stated conditions were selected so that the breaker type became the Spilling breaker.

For each experimental condition, the water surface profile η was measured with capacitance-type wave gages at $0.1L_i$ interval mesh points within the square region of $2.0L_i$ in x-axis and $1.5L_i$ in y-axis, as shown in Fig. 1. The horizontal water particle velocities u and v at three different depths on each mesh point were also measured with electromagnetic type velocimeters. Moreover, the wave breaking process was recorded using a video tape recorder.

NUMERICAL CALCULATION METHOD

A numerical model has been developed to study the wave breaking process due to the submerged breakwater in the three-dimensional wave field (Kawasaki, 1998). The model utilizes a SOLA-VOF method (Hirt and Nichols, 1981) as well as a non-reflective wave generator (Brorsen and Larsen, 1987). Further, an added dissipation zone is adopted to treat the open boundaries (Hinatsu, 1992).

The wave field is governed by the continuity equation (Eq.(2)) and Navier-Stokes equations (Eq.(3) \sim (5)) for incompressible fluid. The free surface is treated by introducing a function F that represents the fractional volume of the cell occupied by the fluid, as in Eq.(6).

$$\frac{\partial u}{\partial x} + \frac{\partial v}{\partial y} + \frac{\partial w}{\partial z} = q = \begin{cases} q^* / \Delta x_S & \text{at } x = x_S \\ 0 & \text{at } x \neq x_S \end{cases}$$
(2)

$$\frac{\partial u}{\partial t} + u\frac{\partial u}{\partial x} + v\frac{\partial u}{\partial y} + w\frac{\partial u}{\partial z} = -\frac{1}{\rho}\frac{\partial p}{\partial x} + \nu\nabla^2 u \tag{3}$$

$$\frac{\partial v}{\partial t} + u\frac{\partial v}{\partial x} + v\frac{\partial v}{\partial y} + w\frac{\partial v}{\partial z} = -\frac{1}{\rho}\frac{\partial p}{\partial y} + \nu\nabla^2 v + \frac{\nu}{3}\frac{\partial q}{\partial y}$$
(4)

$$\frac{\partial w}{\partial t} + u\frac{\partial w}{\partial x} + v\frac{\partial w}{\partial y} + w\frac{\partial w}{\partial z} = -g - \frac{1}{\rho}\frac{\partial p}{\partial z} + \nu\nabla^2 w + \frac{\nu}{3}\frac{\partial q}{\partial z} - \gamma w \qquad (5)$$

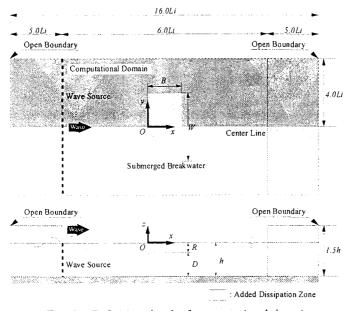


Fig. 2 Definition sketch of computational domain

$$\frac{\partial F}{\partial t} + \frac{\partial (Fu)}{\partial x} + \frac{\partial (Fv)}{\partial y} + \frac{\partial (Fw)}{\partial z} = Fq \tag{6}$$

where the Cartesian coordinate system (x,y,z) is used. u, v and w are the velocity components in respective direction of x, y and z. q is the wave generation source with its strength $q^*/\Delta x_S$ only assigned at source line $(x=x_S)$, in which q^* is twice horizontal velocity component of the generated wave (the third-order Stokes wave in this study), and Δx_S is the mesh size in x-direction at $x=x_S$. tis the time, p the pressure, ρ the fluid density, ν the kinematic viscosity, g the gravitational acceleration, and $\nabla = (\partial/\partial x, \partial/\partial y, \partial/\partial z)$. γ is the positive wave dissipation factor and equals 0 except for the added dissipation zone.

As shown in Fig. 2, the computational domain (shaded portion) is the half side of total region because it was confirmed from laboratory experiments that the wave breaking phenomenon was almost symmetrical for the center line of the submerged breakwater. The computational domain is $16.0L_i \times 4.0L_i \times 1.5h$ in the respective directions of x, y and z. The positive x-direction is onshoreward. The vertical z-axis is taken positive upward with its origin being on the still water level. The mesh sizes Δx , Δy and Δz are

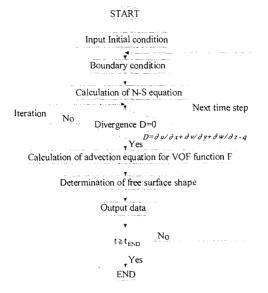


Fig. 3 Flow chart of numerical calculation

 $1/50L_i$, $1/50L_i$ and 1/40h in respective directions of x, y and z. The time interval Δt is kept constant at 0.001s so as to satisfy the Courant condition at every time step.

The flow chart of the present numerical scheme is shown in Fig. 3. The Navier-Stokes equations (Eqs.(3) \sim (5)) are used to calculate the first approximation of the velocities at the next time step. However, the calculated velocities do not satisfy, in general, the continuity equation Eq.(2). Therefore, to satisfy the continuity equation completely, the velocities and the pressure are repeatedly adjusted. Next, using the thus obtained velocities, the behavior of the free-surface is evaluated by calculating the advection equation Eq.(6).

Stable numerical computation is carried out by repeating the abovementioned procedures under suitable boundary conditions at each time step.

RESULTS AND DISCUSSIONS

(a) Breaking Limit, Breaker Types and Breaking Position

Figure 4(a) and (b) illustrate the critical relative wave height for the wave breaking $(H_i/L_i)_c$ or $(H_i/R)_c$ in relation to the relative structure length W/L_i , in which $W/L_i=\infty$ means the two-dimensional experimental results

(Iwata et al., 1996). The breaking limit Eq.(7) at the constant depth derived by Miche (1944) is also shown for comparison. In this study, the wave breaking is defined as the instance when the wave front became vertical.

$$\left(\frac{H_i}{L_i}\right)_c = 0.142 \tanh\left(\frac{2\pi h}{L_i}\right) \tag{7}$$

The wave breaking first occurs, in general, at both side edges of the submerged breakwater and then spreads, with wave propagation, to the onshore center line of the structure. As shown in Fig. 4(a) and (b), W/L_i little effects the breaking limit under $1.0 \leq W/L_i \leq 2.5$. According to Fig. 4(b), the critical relative wave height $(H_i/R)_c$ is 0.35 for $h/L_i=0.2$ and 0.41 for $h/L_i=0.4$, which are smaller than their respective two-dimensional values $(W/L_i=\infty)$; $(H_i/R)_c \cong 0.39$ for $h/L_i=0.2$ and $(H_i/R)_c \cong 0.49$ for $h/L_i=0.4$. In other words, the wave in three-dimensional wave field is likely to break under smaller incident wave height than the case of two-dimensional field. This is thought to be largely attributed to the wave refraction by the abrupt change of water

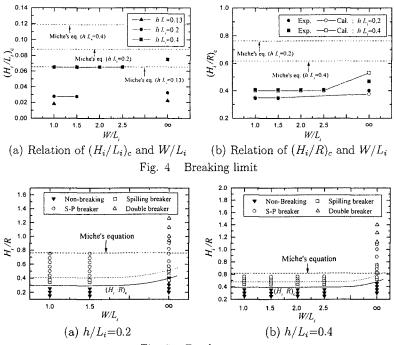
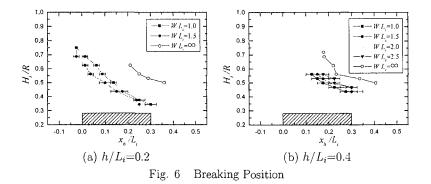


Fig. 5 Breaker types



depth. Figure 4(b) also indicates that the breaking limit calculated with the present numerical calculation method coincides with experimental values.

Laboratory experiments reveal, as shown in Fig. 5, that the breaker types are classified into Spilling breaker (\Box), S-P breaker which means an intermediate type between Spilling and Plunging breakers (\bigcirc), and Double breaker (\triangle). The Double breaker is defined as twice breaking in front of and above the structure due to the wave-induced return flow (Katano et al., 1992). It is also found out from Fig. 5 that regardless of W/L_i , the breaker type changes from Spilling to S-P breaker with an increment of H_i/R under $0.5 \leq W/L_i \leq 2.5$. The occurrence range of each breaker type can be graphically given in Fig. 5(a) and (b). This would show that the magnitude of the wavesubmerged breakwater interaction becomes smaller with an increment of h/L_i .

Figure 6 shows the relationship between x_b/L_i and H_i/R with parameter of W/L_i in case of $h/L_i=0.2$ and 0.4, where x_b is the distance from the front face of the submerged breakwater to the breaking point. Regardless of W/L_i , the breaking point shifts to the offshore side with an increase of H_i/R . In Fig. 6(a), $x_b/L_i=-0.05$ is attained for $H_i/R \ge 0.7$ because of forming the partial standing wave. Moreover, the breaking point in the three-dimensional case shifts to the offshore side as compared with the two-dimensional case.

(b) Wave Deformation

Figure 7 indicates one example of the wave height distribution, in which the breaker type is a weak Spilling breaker. The wave height above the submerged breakwater becomes larger than the incident wave height $(H/H_i \ge$ 1.0), especially the wave height at the side edge of the submerged breakwater $(y/L_i=0.3)$ is much larger.

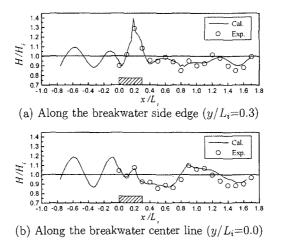


Fig. 7 Comparison of wave height variation between computation and laboratory experiment $(H_i/L_i=0.05, h/L_i=0.2, W/L_i=1.0)$

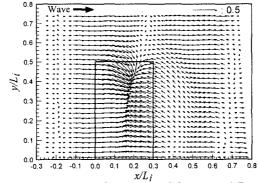


Fig. 8 Water Particle Velocity around Submerged Breakwater $(h/L_i=0.2, H_i/L_i=0.05, W/L_i=1.0; z/h=-0.15, t/T_i=7.0)$

The reason of this can be explained from Fig. 8, which shows the water particle velocity at z/h=-0.15 when the free-surface at the side edge of the structure becomes extremely large. According to this figure, the direction of the velocity is converged near the side edge of the structure due to the wave refraction by an abrupt change of the water depth. Therefore, as already mentioned, it can be thought that the wave height at the side edge of the submerged breakwater becomes extremely large mainly by the effect of the wave refraction.

As shown in Figs. 7 and 9, the water surface profiles as well as the wave height before and after wave breaking, computed with the present numerical calculation method, are in good agreement with those of the laboratory experiments. In addition, as shown in Fig. 10 (the case of a weak Spilling breaker), the computed water particle velocities agree well with the experimental values. Therefore, the present numerical calculation method can evaluate well the breaking wave deformation in case of the Spilling breaker.

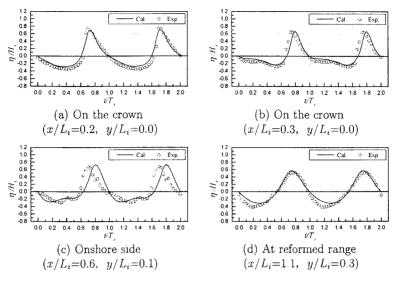
The calculation results, as demonstrated in Fig. 11, reveals that the diffracted wave is generated around the structure and that the partial standing wave is formed in front of the structure. It is also found that the relative structure length W/L_i affects the wave height above the structure.

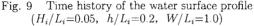
(c) Wave Spectra

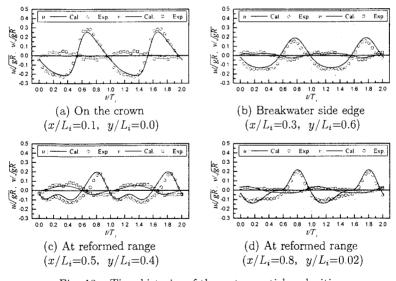
Figure 12 shows the spatial distribution of the non-dimensional wave height spectrum $2A(f)/H_i$, where A(f) is the amplitude spectrum and f is the wave frequency. It is obvious that the decreasing region of the fundamental harmonic component coincides with the increasing region of the second harmonic component. This would indicate the shift of the wave energy of the fundamental harmonic component to that of the second harmonic component. The fundamental harmonic component increases again in the range of the non-breaking reformed wave (roughly $x/L_i \ge 1.0$), while the second harmonic component is decaying with wave propagation. The amplitude variation of the second harmonic component is seen to be periodic at the onshore side of the structure. Therefore, similar to Massel's results (1983) for non-breaking waves in two-dimensional wave field, it can be judged that the free second harmonic component wave is generated even under the condition of wave breaking.

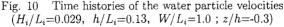
(d) Mean Velocity Field

Figure 13 shows the numerical and experimental results for the mean velocity field around the submerged breakwater. It is recognized from Fig. 13(i) and (ii) that there is the strong mean onshore velocity near the free-surface at onshore side of the submerged breakwater. This is due to the wave breaking above the submerged breakwater. The mean offshore velocity, i.e. the return flow is also found to be caused near both the side of the structure (0.5 $\leq y/L_i \leq 1.0$) and the bottom. Thus, it is clear that the return flow takes place to compensate the onshore mass transport around the still water level caused by wave breaking. Judging from the above-stated, it can be said that









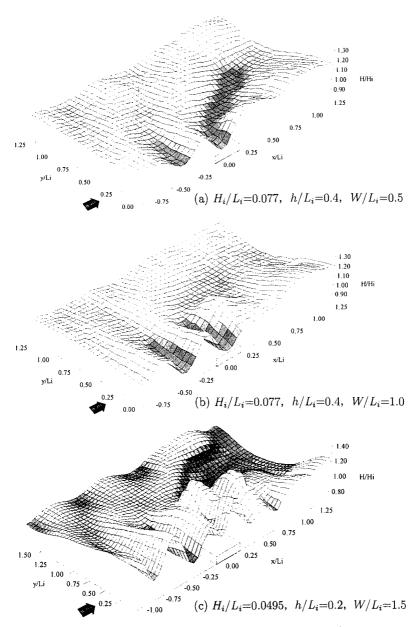


Fig. 11 Spatial distribution of computed wave height around structure

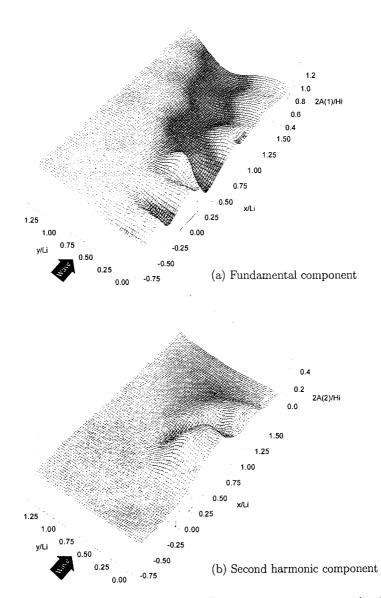
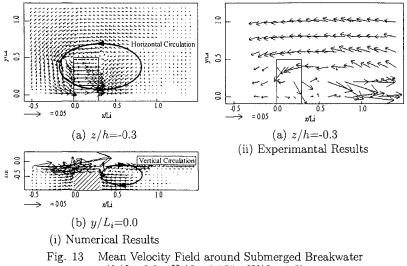


Fig. 12 Computed spatial distribution of Fourier component wave amplitude $(h/L_i=0.2, H_i/L_i=0.05, W/L_i=1.0)$



 $(h/L_i=0.2, H_i/L_i=0.055, W/L_i=1.0)$

two circulation flows, that is, the horizontal and vertical circulation flows are formed around the submerged breakwater.

CONCLUSIONS

Main conclusions in this study are summarized as follows:

- 1) The breaking limit and the breaker types are almost independent of the relative structure length W/L_i in the range of $0.5 \le W/L_i \le 2.5$.
- 2) The breaker type changes from Spilling to an intermediate breaker between Spilling and Plunging breakers (S-P breaker) with an increment of the relative incident wave height H_i/R .
- 3) The breaking position shifts to the offshore side as H_i/R becomes larger.
- 4) The free second harmonic component wave is possibly generated from the edge side of the submerged breakwater.
- 5) The horizontal and vertical circulation flows are formed around the submerged breakwater.
- 6) The present numerical calculation model with the SOLA-VOF method has been found to evaluate well the wave deformation before and after breaking in case of weak breakers like the Spilling breaker.

REFERENCES

- Brorsen, M. and Larsen, J.(1987). "Source generation of nonlinear gravity waves with boundary integral equation method", *Coastal Eng.*, Vol. 11, pp. 93-113.
- Goda, Y.(1983). "Description of wave nonlinearity with a unified parameter", Proc. 30th Japanese Conf. on Coastal Eng., pp.39-43 (in Japanese).
- Hinatsu, M.(1992). "Numerical simulation of unsteady viscous nonlinear waves using moving grid system fitted on a free surface", J. Kansai Soc. Naval Architects Japan, No.217, pp.1–11.
- Hirt, C.W. and Nichols, B.D.(1981). "Volume of Fluid (VOF) method for the dynamics of free boundaries", J. Comp. Phys., Vol. 39, pp.201-225.
- Iwata, K., K. Kawasaki and D.-S. Kim(1996). "Breaking limit, breaking and post-breaking wave deformation due to submerged structures", Proc. of 25th ICCE, ASCE, Vol.2, pp.2338-2351.
- Katano, A., S. Murakami and M. Hattori(1992). "Relevant parameters representing energy dissipation due to submerged breakwaters", Proc. Coastal Eng., JSCE, Vol. 39, pp. 646–650 (in Japanese).
- Kawasaki, K.(1998). "Fundamental study on wave breaking and post-breaking deformation due to submerged structure", *Dissertation, Nagoya Univer*sity, 186p (in Japanese).
- Massel, S.R. (1983). "Harmonic generation by waves propagating over a submerged step", Coastal Eng., Vol. 7, pp.357–380.
- Miche, A.(1944). "Mouvements ondulatories de la mer en profendeur constante ou decroissante, forme limit de la houle lors de som déferlement", *Application aux digues maritimes, Ann. Ponts et Chausees*, Tome 114 (in French).
- Petit, H.A.H., P. Tönjes, M.R.A. van Gent and P. van den Bosch(1994). "Numerical simulation and validation of plunging breakers using a 2D Navier-Stokes model", Proc. 24th ICCE, ASCE, Vol.1, pp.511–524.
- Sabeur, Z.A., N.W.H. Allsop, R.G. Beale and J.M. Dennis(1996). "Wave dynamics at coastal structures : Development of a numerical model for free surface flow", Proc. 25th ICCE, ASCE, Vol.1, pp.389-402.
- van Gent, M.R.A., Tönjes, H.A.H. and van den Bosch, P.(1994). "Wave action on and in permeable structure", Proc. 24th ICCE, ASCE, Vol. 2, pp.1739-1753.